



Cite this: DOI: 10.1039/d1sm01515j

Spontaneous formation of anisotropic microrods from paraffin wax in an aqueous environment†

Wei Wang,^a Jianguo Wen, Elena Shevchenko ^a and Xuedan Ma ^{a*}

The construction of functional nano-/micro-architectures through self-assembly and self-organization of organic molecules and polymeric materials plays an important role in the development of many technologies. In this study, we report the spontaneous formation of uniform polymer microrods with lengths of up to a few tens of micrometers from paraffin wax. Through a solvent attrition approach, colloidal structures of paraffin wax are introduced into water. After the initial growth stage, the microrods undergo morphological transformation and end-to-end aggregation, processes likely driven by thermodynamics to create equilibrium structures with minimal interfacial energies. The polymer microrods can effectively absorb hydrophobic nanoparticles, indicating their potential to serve as host materials for functional components. The formation of polymer microrods from paraffin wax and their spontaneous growth mechanism discovered in this study may provide new insights to the self-assembly of microstructures.

Received 20th October 2021,
Accepted 24th November 2021

DOI: 10.1039/d1sm01515j

rsc.li/soft-matter-journal

1 Introduction

The formation of one-dimensional (1D) nano- and microstructures from organic molecules^{1,2} and polymers^{3,4} have attracted great attention due to the unique optical, electronic, and magnetic properties offered by the resultant structures, that may enable their potential applications as building blocks for miniaturized optoelectronic devices and catalytic systems. 1D microrods have also been proposed to be candidates as biologically active materials for drug delivery^{5,6} and model systems for studying the phase behavior of liquid-crystal forming structures.^{7,8}

Combining elements of molecular design and self-assembling conditions, organic molecules can stack orderly and form 1D structures through intermolecular interactions such as hydrogen bonding, electrostatic, hydrophobic, and π - π stacking interactions.^{9–12} In comparison, self-assembly of polymers into 1D structures typically relies on the controlled formation of micelles from amphiphilic polymers composed of hydrophilic and hydrophobic units. The formed micelles consist of insoluble blocks as the cores and soluble blocks as the coronas.^{13,14} The self-assembled 1D polymer fibers typically have core widths on nanometer scales, corresponding approximately to the width of the micelles. The lengths of the polymer fibers can extend up to micrometers, depending on the chemical

nature of the polymers and self-assembling conditions.^{14,15} Similar to the self-assembly of organic molecules, the growth processes of polymers are governed by enthalpic and entropic contributions to the aggregate formation.^{13,16}

Alternatively, polymer microrods have been prepared through a shear flow-solvent attrition process,^{4,7,17} during which polymer droplets are injected into viscous media and broken up by shear forces. The solvent attrition and subsequent precipitation and solidification of the polymers can result in high aspect ratio microrods that are tens to hundreds of micrometers in length. Unlike self-assembly of polymers that is driven by thermodynamic profiles, this approach relies on external parameters such as shear rate and media viscosity in controlling the morphologies of the polymer microrods.

Here, we report the spontaneous formation of uniform polymer microrods with high aspect ratios from paraffin wax using the combination of solvent attrition and polymer self-assembly. Paraffin wax, the main composition of Parafilm, is inexpensive and extensively used in laboratories for sealing and protection due to their good mechanical properties and chemical inertness. Paraffin wax has a complex composition but mainly consists of low molecular weight polyethylene and has a melting temperature of around 60 °C.^{18,19} It has been used as encapsulating matrix to protect conjugated semiconductor polymers in optoelectronic devices²⁰ and as channel materials for microfluidic devices.¹⁹ Paraffin wax has also been used for loading functional nanoparticles to obtain prescribed properties.²¹ In this study, we demonstrate that using a liquid–liquid dispersion method and the subsequent self-assembly process, polymer microrods can be formed from paraffin wax in

^a Center for Nanoscale Materials, Argonne National Laboratory, Lemont, Illinois 60439, USA

^b Consortium for Advanced Science and Engineering, University of Chicago, Chicago, Illinois 60637, USA. E-mail: xuedan.ma@anl.gov

† Electronic supplementary information (ESI) available. See DOI: 10.1039/d1sm01515j

an aqueous environment. By monitoring the time-dependent morphologies of the microrods, we find that their formation process is directed by thermodynamics and likely involves three major steps: the formation of microrod seeds, the growth and elongation of the microrods, and the end-to-end aggregation of the microrods. Interestingly, the formed microrods can absorb nanoparticles that are dissolved in organic solvents efficiently, rendering their potential applications for loading optically and catalytically active materials.

2 Experimental section

2.1 Materials and chemicals

Acetone ($\geq 99.5\%$, Sigma-Aldrich), isopropanol ($\geq 99.5\%$, Sigma-Aldrich), Parafilm (Heathrow Scientific), and CdSe/ZnS core-shell quantum dots in toluene (Sigma-Aldrich) were purchased and used as received. Distilled water ($18.2\text{ M}\Omega$; Millipore Co.) was used in all experiments.

2.2 Self-assembly of polymer microrods

All the glassware used in the study was thoroughly cleaned and dried to prevent any contamination. To initiate the formation of the polymer microrods, a 1 cm by 1 cm Parafilm was added to a mixture of acetone and isopropanol. The volume ratio between the acetone and isopropanol was varied between 1:10 to 10:1, although no noticeable changes in the formation of the microrods was observed. The suspension was sealed and ultrasonicated for 30 minutes in a bath sonicator, after which the remaining undissolved Parafilm was taken out. 0.01–1 mL of the resultant suspension was added to 10 mL of distilled water. It is worth mentioning that when the ratio between the Parafilm suspension and water is too high, irregular polymeric structures instead of uniform microrods were eventually observed over time, indicating a separate phase being formed in the water when the polymer mixture concentration is high. The mixture was ultrasonicated for another 60 minutes and appeared to be clear and transparent. At the end of the ultrasonication, a noticeable increase in the bath temperature can be detected. The final product was kept in ambient conditions for designated amounts of time.

2.3 Characterization

The morphologies of the microrods were monitored using optical microscopy (Nikon Eclipse LV100ND), scanning electron microscopy (SEM, JOEL JSM-7500F), and transmission electron microscopy (TEM, FEI Titan 80–300). The compositions of the microrods were investigated by energy dispersive X-ray spectroscopy (EDS) in combination with SEM and electron energy loss spectroscopy (EELS). High-resolution TEM was used to determine the crystalline structures of the microrods. Samples for these studies were prepared by drying droplets of the aqueous suspensions on pre-cleaned substrates or TEM grids.

To study the integration properties of the polymer microrods with functional nanomaterials, we spin coat CdSe/ZnS core-shell quantum dots dispersed in toluene onto microrods

that were pre-dried on substrates. The photoluminescence properties of the resultant structures were investigated using a confocal laser scanning microscope. Pulses from a diode laser with a frequency of 1 MHz and a wavelength of 400 nm were focused onto the samples using a microscope objective ($40\times$, $\text{NA} = 0.95$). Emission from the samples was collected by the same objective and sent to single photon avalanche diodes for scanning photoluminescence imaging or a 500 mm spectrometer equipped with a charge-coupled device for spectroscopic studies.

3 Results and discussion

Fig. 1a and b show representative optical micrographs of the polymer microrods formed in water after 19 and 82 days, respectively. The microrods appear to be relatively uniform in diameter and length, and a noticeable increase in their lengths over aging time can be observed. SEM images of the microrods shown in Fig. 1c and d give consistent structural information. The compositions of the microrods are determined by performing EDS measurements. As shown in Fig. 1e and f, the major composition of the microrods is carbon, confirming their polymeric nature. The apparent peak corresponding to silicon in the EDS spectrum is caused by the underlying substrates. Control experiments of EDS measurements on blank silicon substrates and paraffin wax (S1, ESI[†]) indicate that the small trace of oxygen observed in the microrod samples likely has major contributions from the native layer of SiO_2 on the silicon substrate surface, although the microrods may also contain a small percentage of oxygen.

Our EELS analyses of the microrods further confirm our assignments of the major compositions (Fig. 1g and h). The EELS spectra of the microrods show predominant signatures from amorphous carbon, which include a carbon K-edge peak starting at 289 eV and a small low-energy pre-peak at around 284 eV. The former can be assigned to core $\rightarrow \sigma$ electronic transitions in carbon and the latter is commonly associated with unsaturated π states.^{22,23} A weak peak can also be observed at the oxygen K-edge (Fig. 1h), indicating the existence of a small percentage of oxygen in the microrods, consistent with the EDS measurements. We further study the structural properties of the microrods using high-resolution TEM (Fig. 1i and j). The lack of sharp ring patterns in their electron diffraction (Fig. 1j, inset) indicates their amorphous nature. These analytical results confirm that the microrods are composed of paraffin wax which is mostly low molecular weight polyethylene.^{18,19}

Solvent attrition has previously been used as an effective approach in inducing polymer precipitation in nano-/macro-scale droplets.^{4,7,24} Analogous to the liquid antisolvent precipitation process, it involves the addition of an antisolvent, which is a non-solvent for the polymer but miscible with the solvent, to the polymer solution. The liquid–liquid dispersion between the solvent and antisolvent decreases the solubility of the polymer in the solution and leads to its precipitation. Depending on the external force used to define the droplet shape and volume,

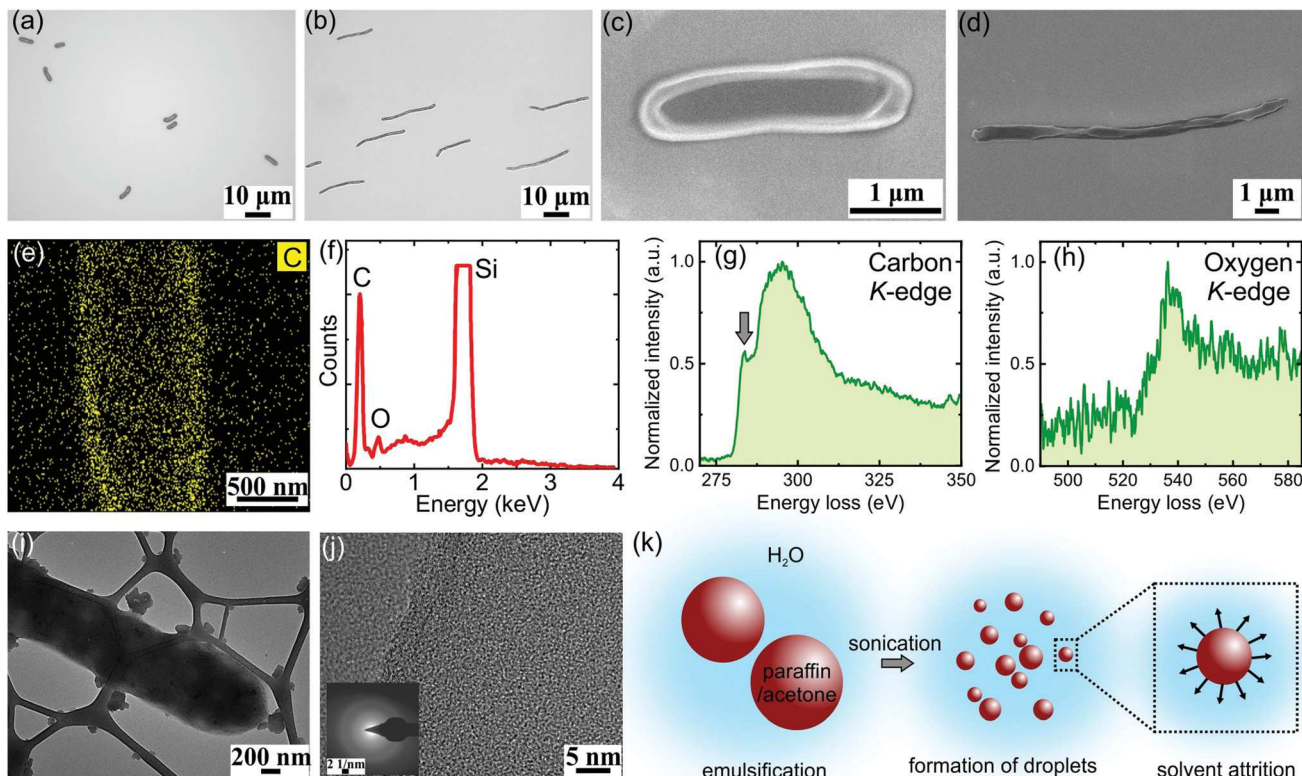


Fig. 1 (a) and (b) Optical micrographs of representative microrods after growing for 19 days and 82 days, respectively. (c) and (d) SEM images of representative microrods after growing for 12 days and 82 days, respectively. (e) and (f) EDS mapping of carbon and the corresponding EDS spectrum of a microrod. The apparent peak corresponding to silicon is caused by the substrate. (g) and (h) EELS spectra of the microrods at the carbon and oxygen K-edges. (i) and (j) TEM images of a microrod. Inset in (j) is a representative electron diffraction pattern (SAED pattern) of a microrod. (k) Schematic of the solvent attrition method leading to the formation of the microrod seeds.

the rates of solvent-non-solvent mixing, and the solidification speed of the polymers, spherical nanoparticles,^{24,25} microrods,^{4,7} and dendritic microparticles²⁶ have been fabricated.

We believe that the initial formation process of the polymer microrods observed in our study can be attributed to a similar mechanism. Specifically, we start by dissolving the paraffin wax in acetone.²⁷ When the paraffin/acetone solution is added to water subject to ultrasonication, three concurrent processes occur: emulsification of the paraffin/acetone solution in water, ultrasonification-assisted breakdown of the emulsion into small droplets, and diffusion of acetone out of the droplets, leaving behind the paraffin wax because it is not soluble in water (Fig. 1k). The interdiffusion of acetone and water (the so-called solvent attrition) reduces the solubility of the paraffin wax, leading to its precipitation in the droplets, forming colloidal scale features. Our TEM studies of the paraffin wax solutions right after their preparation confirm this assumption (see S2 for TEM images of the initially formed nanoparticles, ESI†). During these processes, droplet coalescence and post-precipitation agglomeration of the polymers could also occur.²⁵ We believe these precipitated polymers with colloidal scale structures to be the initial seeds for the growth of the microrods, and they are still visible in the later stages of the microrod growth (see *e.g.* the small particles in Fig. 1i). According to the solvent attrition mechanism, it is potentially possible to control

the size and morphology of these seed materials by altering the miscibility of the polymer solvents with water. Future detailed studies in this direction would help improve the control over the microrod morphology.

However, deviating from the previously reported solvent attrition methods, in which the final forms of the microstructures were consolidated by immediate UV light-induced polymer crosslinking,^{4,7,26} the liquid–liquid dispersion process in this study only creates the initial seeds for the microrods that would subsequently undergo a slow, spontaneous self-assembly process over a long period of time. This is evident by the increase in the lengths of the microrods over aging time, as shown in Fig. 1a–d. To further understand the growth mechanism of the microrods, we study their time-dependent morphology. Fig. 2a–e show images of the microrods after they have grown for various periods of time in aqueous solutions. The corresponding histograms of their length distributions are plotted in Fig. 2f–j. At the early stages, short microrods that are a few micrometers long and with narrow length distributions can be observed (Fig. 2a, b, f and g). Continued growth of the microrods can be observed in the next few weeks during which their lengths increase up to a few tens of micrometers (Fig. 2c–e). Interestingly, there seems to be an intermediate growth stage when primarily two species of microrods with distinct lengths can be observed, as shown in Fig. 2c, d, h and i, with the average length

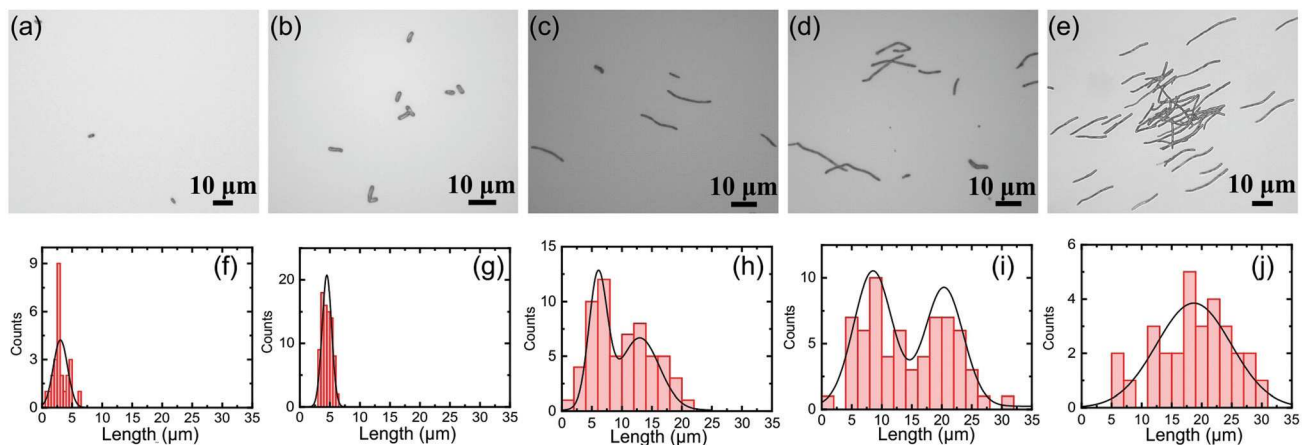


Fig. 2 (a)–(e) Optical micrographs of the microrods after growing for 12 (a), 19 (b), 39 (c), 55 (d) and 82 (e) days, respectively. (f)–(j) The corresponding histograms of the microrod lengths. Curves are Gaussian fits to the histograms.

of one species being around 2–3 times that of the other species. Over time, they evolve into one species of microrods with broad length distributions (Fig. 2e and j).

To better quantify the growth mechanisms of the microrods, we plot their average lengths and widths as a function of time in Fig. 3a. For clarity, we arbitrarily divide their growth process into four different stages. With an increase in the growth time, the originally nanometer sized nanoparticles aggregate and grow into elongated structures, with the length of the microrods increasing monotonically first (stages I–III) until it reaches

a plateau (stage IV), potentially caused by the exhaust of source materials in the solutions or equilibrium structures reached. It is possible that as the microrods become longer, their diffusivity might decrease. This reduced diffusivity may also contribute to the observed plateau due to the lower probability of the microrods encountering additional source materials or other microrods. We note that it remains unclear how the initial spherical nanoparticles assemble into the isotropic, elongated structures observed in stage II. More studies are needed to understand the underlying mechanism in this process.

From the standard errors of the average length values, it can be inferred that there is an increase in the length distribution during the intermediate and late growth stages (stages III and IV), which is consistent with the two distinct species of microrods observed in Fig. 2h and i. In parallel, the corresponding widths of the microrods first increases and then decreases, after which it stays constant. To identify if there are correlations between the changes in the lengths and widths of the polymer microrods, we plotted three representative cases in Fig. 3b–d, each representing a growth stage from II to IV, respectively. As can be seen in Fig. 3b, at the early growth stage II, the microrods are relatively short and thick. As they continue to grow, the short, thick microrods start to turn into long but thin ones (Fig. 3c), with the length of the latter ranging from about 1 to 3 times that of the former. Eventually, all the microrods evolve into thin elongated shapes with significantly increased aspect ratios (Fig. 3d).

Based on these observations, we speculate that in stage III and IV, two major processes occur: (i) the transformation of the short, thick microrods into long, thin ones, and (ii) the end-to-end assembly of the microrods. The former is supported by the eventual disappearance of the short, thick microrods and the concurrent emergence of the long, thin ones. This morphological transformation of the polymer microrods reflects their “living self-assembly” nature, a phenomenon that is likely due to the transfer of materials within the microrods until an equilibrium structure is achieved. We speculate this mass transport-induced geometrical transformation might be related to the rearrangement of chemical compositions¹⁵ with

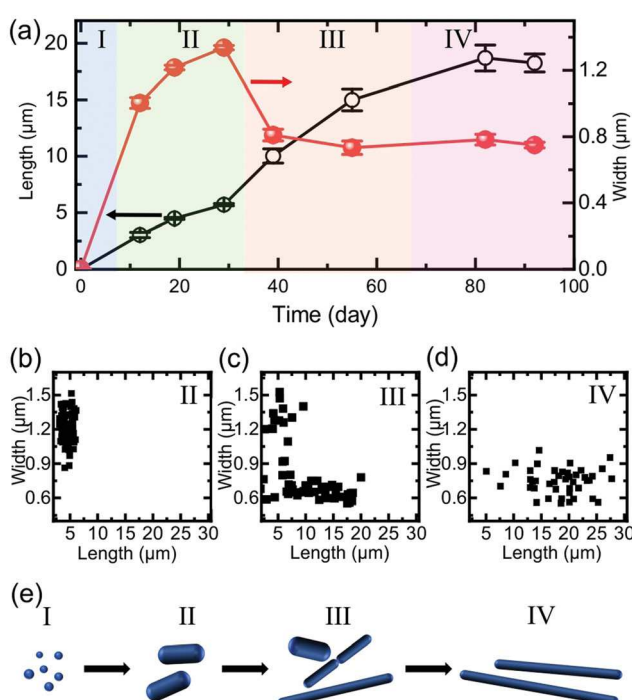


Fig. 3 (a) The time-dependent lengths (black circles) and widths (red dots) of the microrods. (b)–(d) The morphology of the microrods in growth stages of II (b), III (c) and IV (d) represented by plotting their lengths versus widths. (e) A sketch of the microrod growth process.

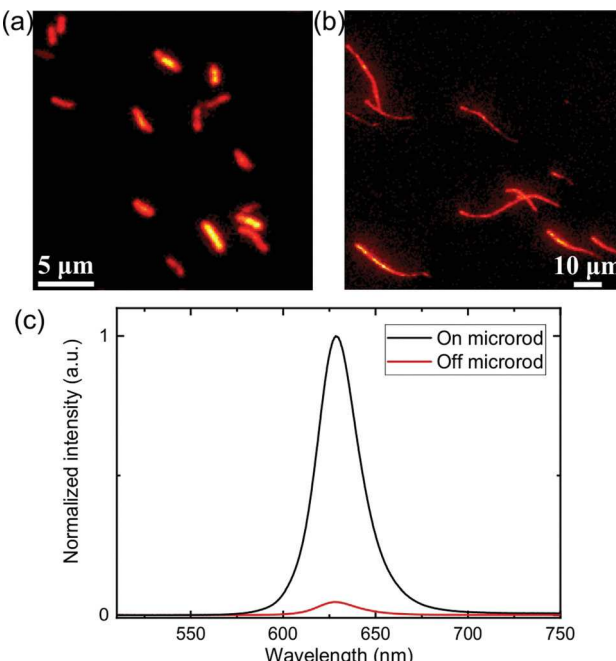


Fig. 4 (a) and (b) Scanning photoluminescence images of short (a) and long (b) microrods from two different growth stages spin coated with quantum dots. (c) Photoluminescence spectra taken from the microrods and from the adjacent background area.

hydrophobic parts moving towards the interiors of the microrods, and/or the tendency of the microrods to form energetically favorable surface curvatures. Future studies by applying this approach to homo- and co-polymers with varying well-defined chemical compositions would help shed light on the underlying mechanisms. The living self-assembly nature of the microrods is further supported by the drastic acceleration in their growth rates when additional paraffin source materials were added to the suspensions at a late growth stage (see Fig. S3, ESI†), indicating the potential for continued growth of the microrods.

Our derivation of the end-to-end assembly of the microrods is supported by the coexistence of two distinct types of microrods with the length of one species being around 2–3 times that of the other species, and our occasional observation of such end-to-end microstructures (S4, ESI†). When two to three of the microrods encounter one another in solution, they stack end-to-end and grow into one long microrod. We illustrate this growth process in Fig. 3e. Interestingly, the end-to-end growth only happens among microrods of similar diameters. This kind of “epitaxial” aggregation/growth mechanism in which the growth of the cylindrical structures only occurs at the ends has also been observed in the self-assembly of micelles from copolymeric systems,^{15,28} and is typically driven by the affinity of the cylinder ends to minimize their lateral interfacial energies.¹³ We believe a similar mechanism is at play in our system. To reduce the large surface tensions at the microrod ends caused by their large curvatures, the microrods may tend to aggregate by their ends to reduce the overall surface energy.

One of the potential applications of polymer microrods is to serve as hosts of functional components for lighting, drug delivery, and catalytic applications. We explore the possibility of integrating functional nanostructures into the microrods by spin coating semiconductor quantum dot (QD) solutions onto the pre-dried microrods. Bright, uniform photoluminescence can be observed from both the short and long microrods (Fig. 4a and b), with the photoluminescence spectra matching that of the QDs. In comparison, photoluminescence intensity from the adjacent substrate areas is much weaker (Fig. 4c). These observations suggest that the QDs preferentially adsorb onto the microrods, likely due to the hydrophobic nature of the polymer microrods that allow them to serve as “sponges” for absorbing the QDs dissolved in toluene. Additionally, the emission from the incorporated QDs stays constant and stable over a few months’ time. It is likely that due to the nanometer sizes of the QDs and the porosity nature of the microrods, the QDs have penetrated into the interiors of the microrods. Upon encapsulation of the QDs in the paraffin wax which protects them from environmental perturbations, the QDs become more photostable. Due to the post-synthesis integration approach demonstrated here, it is potentially feasible to replace the QD solutions used in this study with other types of functional materials such as plasmonic nanoparticles^{29,30} and light emitting dyes³¹ and load them into the microrods conveniently. Alternatively, it may be possible to introduce functional materials during the solvent attrition step, as was previously demonstrated.³² The rod-like structures such as those observed in this study could be beneficial for miniaturized, flexible optoelectronic devices such as LEDs due to the feasibility to align them longitudinally.^{33,34} Moreover, they may provide new opportunities for surface plasmon-based sensors and light-matter interactions.^{35,36}

4 Conclusions

In summary, we report the spontaneous formation of uniform polymer microrods from paraffin wax in water. Adapting a solution attrition approach, solutions of paraffin wax are introduced to water under ultrasonification, leading to the formation of paraffin precipitates that serve as seeds for the polymer microrods. Our time-dependent morphological studies of the microrods show that after the initial growth stage, the microrods undergo morphological transformation and turn into long and thin structures. In addition, they also self-assemble into end-to-end chain-like structures. These processes combined eventually lead to high aspect-ratio microrods that extend up to a few tens of micrometers in length. The “living self-assembly” nature of the microrods, which resembles those of block copolymer micelles, is likely driven by thermodynamics to minimize their interfacial energies. Due to their hydrophobic nature, the polymer microrods appear to be efficient absorbents for organic nanostructures. We demonstrate the integration of quantum dots in the polymer microrods, leading to bright and homogeneous emission from them. The formation of microrods from paraffin wax and their unique

self-assembly process discovered here may provide new perspectives for the fabrication of functional nano- and micro-structures. Future studies exploring the applicability of this method to various types of polymers would be valuable.

Conflicts of interest

There are no conflicts to declare.

Acknowledgements

We acknowledge support from the National Science Foundation CBET Program under the award no. 2025214. This work was performed, in part, at the Center for Nanoscale Materials, a U.S. Department of Energy Office of Science User Facility, and supported by the U.S. Department of Energy, Office of Science, under Contract No. DE-AC02-06CH11357.

References

- 1 L. C. Palmer and S. I. Stupp, *Acc. Chem. Res.*, 2008, **41**, 1674–1684.
- 2 L. Zang, Y. Che and J. S. Moore, *Acc. Chem. Res.*, 2008, **41**, 1596–1608.
- 3 H. Qiu, Z. M. Hudson, M. A. Winnik and I. Manners, *Science*, 2015, **347**, 1329–1332.
- 4 R. Alargova, K. Bhatt, V. Paunov and O. Velev, *Adv. Mater.*, 2004, **16**, 1653–1657.
- 5 J. Xu, K. Li, M. Liu, P. Li and Y. Fan, *Eur. Polym.*, 2021, **148**, 11037.
- 6 V. P. Chauhan, Z. Popović, O. Chen, J. Cui, D. Fukumura, M. G. Bawendi and R. K. Jain, *Angew. Chem., Int. Ed.*, 2011, **123**, 11619–11622.
- 7 C. Fernández-Rico, T. Yanagishima, A. Curran, D. G. A. L. Aarts and R. P. A. Dullens, *Adv. Mater.*, 2019, **31**, 1807514.
- 8 S. C. Glotzer and M. J. Solomon, *Nat. Mater.*, 2007, **6**, 557–562.
- 9 D. A. Stone, A. S. Tayi, J. E. Goldberger, L. C. Palmer and S. I. Stupp, *Chem. Commun.*, 2011, **47**, 5702–5704.
- 10 Q. Li, Y. Jia, L. Dai, Y. Yang and J. Li, *ACS Nano*, 2015, **9**, 2689–2695.
- 11 Y. Che, H. Huang, M. Xu, C. Zhang, B. R. Bunes, X. Yang and L. Zang, *J. Am. Chem. Soc.*, 2011, **133**, 1087–1091.
- 12 S. Rieth, Z. Li, C. E. Hinkle, C. X. Guzman, J. J. Lee, S. I. Nehme and A. B. Braunschweig, *J. Phys. Chem. C*, 2013, **117**, 11347–11356.
- 13 M. Lazzari and M. A. López-Quintela, *Macromol. Rapid Commun.*, 2009, **30**, 1785–1791.
- 14 C. E. Boott, J. Gwyther, R. L. Harniman, D. W. Hayward and I. Manners, *Nat. Chem.*, 2017, **9**, 785–792.
- 15 L. Shen, H. Wang, G. Guerin, C. Wu, I. Manners and M. A. Winnik, *Macromolecules*, 2008, **41**, 4380–4389.
- 16 P. P. N. Syamala, B. Soberats, D. Görl, S. Gekle and F. Würthner, *Chem. Sci.*, 2019, **10**, 9358–9366.
- 17 A. L. Campbell, B. L. Holt, S. D. Stoyanov and V. N. Paunov, *J. Mater. Chem.*, 2008, **18**, 4074–04078.
- 18 J. Wang, R. Chen, M. Ma and L. Li, *Anal. Chem.*, 2008, **80**, 491–500.
- 19 L. Yu and Z. Z. Shi, *Lab Chip*, 2015, **15**, 1642–1645.
- 20 S. Choi, J. W. Jeong, G. Jo, B. C. Mab and M. Chang, *Nanoscale*, 2019, **11**, 10004–10016.
- 21 J. Wang, H. Xie, Z. Guo and Y. Li, *Appl. Therm. Eng.*, 2014, **73**, 1541–1547.
- 22 *Chemical applications of synchrotron radiation*, ed. T.-K. Sham, World Scientific Publishing Co. Pte. Ltd, Singapore, 2002.
- 23 S. Jung, Y. Myung, B. N. Kim, I. G. Kim, I.-K. You and T. Kim, *Sci. Rep.*, 2018, **8**, 1915.
- 24 X. Zhou, X. Li, T. Mao, J. Zhang and X. Li, *Soft Matter*, 2011, **7**, 6264–6272.
- 25 H. Stewart, M. Golding, L. Matia-Merino, R. Archer and C. Davies, *Colloids Surf. A*, 2016, **498**, 194–205.
- 26 S. Roh, A. H. Williams, R. S. Bang, S. D. Stoyanov and O. D. Velev, *Nat. Mater.*, 2019, **18**, 1315–1320.
- 27 A. P. Grishin and A. P. Kosolapova, *Chem. Technol. Fuels Oils*, 1965, **1**, 362–365.
- 28 T. Gädt, N. S. Ieong, G. Cambridge, M. A. Winnik and I. Manners, *Nat. Mater.*, 2009, **8**, 144–150.
- 29 S. Han, K. Han, J. Hong, D.-Y. Yoon, C. Park and Y. Kim, *ACS Omega*, 2018, **3**, 5244–5251.
- 30 H. Kong and J. Jang, *Chem. Commun.*, 2006, 3010–3012.
- 31 H. Yu and L. Qi, *Langmuir*, 2009, **25**, 6781–6786.
- 32 S. K. Smoukov, T. Tian, N. Vitchuli, S. Gangwal, P. Geisen, M. Wright, E. Shim, M. Marquez, J. Fowler and O. D. Velev, *Adv. Mater.*, 2015, **27**, 2642–2647.
- 33 J.-J. Chiu, C.-C. Kei, T.-P. Perng and W.-S. Wang, *Adv. Mater.*, 2003, **15**, 1361–1364.
- 34 X. Dai, A. Messanvi, H. Zhang, C. Durand, J. Eymery, C. Bougerol, F. H. Julien and M. Tchernycheva, *Nano Lett.*, 2015, **15**, 6958–6964.
- 35 N. Pazos-Perez, T. Borke, D. V. Andreeva and R. A. Alvarez-Puebla, *Nanoscale*, 2011, **3**, 3265–3268.
- 36 X. Ma, H. Tan, T. Kipp and A. Mews, *Nano Lett.*, 2010, **10**, 4166–4174.